

# POST-BAKING LOSSES IN ELECTROPOLISHED NIOBIUM CAVITIES: CUTOUT STUDIES

A. Romanenko\*, G. Wu, L. D. Cooley, Fermilab, Batavia, IL 60510, USA  
G. Ciovati, Jefferson Lab, Newport News, VA 23606, USA

## Abstract

Recent technological advances in superconducting RF (SRF) niobium cavities allowed reaching highest gradients by mitigating the high field Q-slope (HFQS) using the combination of electropolishing (EP) and a 120°C vacuum baking for 24-48 hours. When the high field Q-slope is removed, the hard limit to the achievable accelerating gradients in state of the art cavities is set by the localized quench at surface magnetic fields of 120-200 mT. Nevertheless, localized anomalous losses of different character do still show up in cavity walls, and may lead to the quench at surface fields lower than theoretically possible to sustain. In this contribution we present the first direct study of cavity cutouts representing these lossy areas as well as the quench location in the EP-treated niobium cavity with no HFQS limited by localized quench. Surface studies of cutouts allowed to correlate the post-baking losses with dendritic surface features on the inner cavity surface. The nature and possible origins of these objects is discussed in the context of cavity surface treatments. Possible sources of the high field quench at the corresponding cutout are investigated as well.

## INTRODUCTION

Superconducting radio frequency (SRF) cavities serve as primary particle accelerating structures in many modern accelerators as well as are a technology of choice for several future accelerators. Intense research in recent years has been focused on understanding and overcoming limitations on the way to achieve higher accelerating gradients such as the high field Q-slope and quench. Among different experimental techniques a very powerful approach is provided by using temperature mapping of outside cavity walls during RF tests. Temperature maps allow identifying areas of different dissipation as well as localizing the quench site. Subsequent cutting out areas of interest and subjecting them to extensive surface analytical and superconducting measurements makes possible identifying the differences in near-surface properties leading to different RF dissipation. Such studies have been performed on the high field Q-slope cutouts [1, 2, 3, 5, 6] and low field quench sites [7]. Yet none of the cutout studies have been reported so far on the high field quench and post-baking dissipation, which is currently the practical limit in SRF cavity performance.

We pursued the cutout approach on the mild baked EP niobium cavity free of the high field Q-slope and limited

by the localized quench at the peak surface magnetic field of 160 mT.

## EXPERIMENTAL

### RF Test and Cutout Procedure

An elliptical single cell TESLA shape 1.3 GHz niobium cavity of 2.8 mm wall thickness and 50  $\mu\text{m}$  grain size manufactured by AES was subjected to 105  $\mu\text{m}$  buffered chemical polishing (BCP) followed by 65  $\mu\text{m}$  electropolishing (EP), 120°C vacuum baking for 48 hours and high pressure water rinsing (HPR) before RF tests. The final RF test of the cavity was performed at Jefferson Lab with the temperature mapping system of 576 thermometers attached to the outside cavity walls registering local temperature increase with respect to the bath temperature sensor. The detailed design of the system is described in [8]. The measured quality factor dependence on the peak surface magnetic field at  $T = 2\text{ K}$  is shown in Fig. 1. The maximum

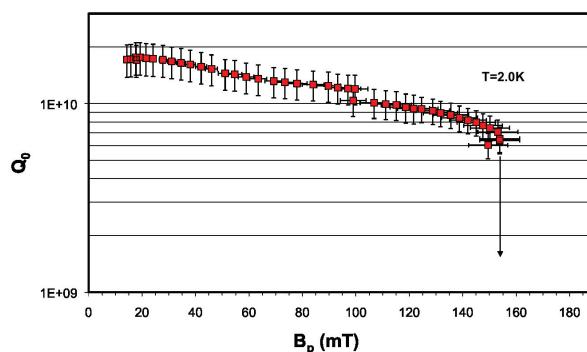


Figure 1: The quality factor  $Q_0$  of the cavity plotted against the peak surface magnetic field  $H_{peak}$  as measured during the RF test.

surface magnetic field was limited by the localized quench at about 160 mT. Temperature maps obtained just before and right after quench are showed in Fig. 2.

Based on these temperature maps three different kinds of locations were identified: (i) exhibiting strong RF losses (black circles in Fig. 2a), (ii) exhibiting weak losses (blue circles), and (iii) the quench site (black circle in Fig. 2b).

Circular samples of about 1 cm in diameter were extracted from the selected locations using the automated milling machine with no lubricant to prevent possible contamination. The rotation speed of the milling tool was kept

\*aroman@fnal.gov

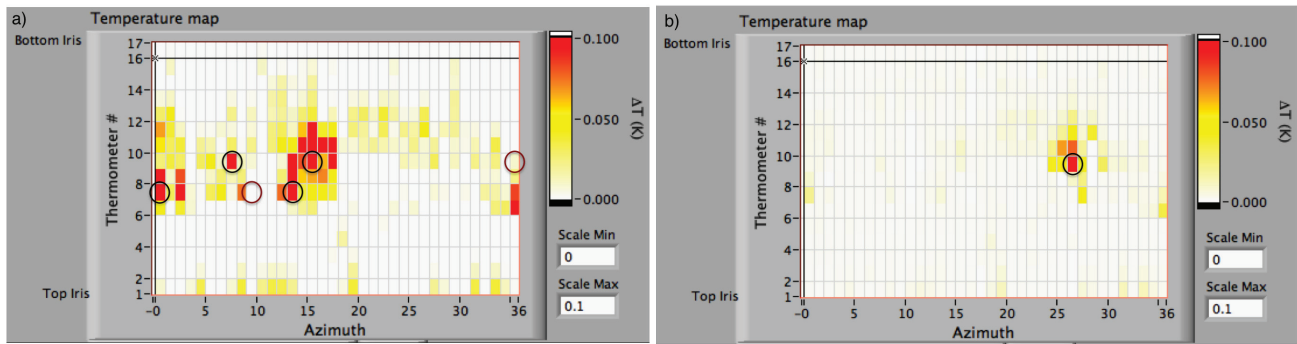


Figure 2: Temperature maps at  $H_{peak} = 160\text{ mT}$  right before (a) and after (b) quench. Locations from where the samples were extracted are marked with black circles for hot spots and quench location, and brown circles for sites with negligible RF losses (cold spots).

low to prevent heating of the sample. A typical cutout sample is shown in Fig. 3 along with the ruler for scale.

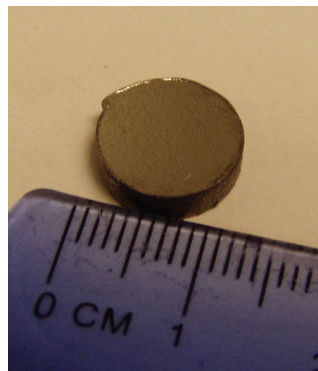


Figure 3: Typical cutout sample extracted from cavity walls. A ruler is shown for comparison.

*Lossy Areas*

Typical individual temperature sensor readings at hot and cold spots are shown in Fig. 4. A series of investigations was performed on each of the samples to elucidate possible surface structure differences leading to the different RF losses. SEM investigation at different electron accelerating voltages uncovered dendritic structures ranging in size from 1 to 15  $\mu\text{m}$  in two hot spots exhibiting the strongest heating. SEM images for the hot spots 130-7 and 150-10 are shown in Fig. 5 and Fig. 6 respectively. One can see that both of the samples have regions covered with dendritic precipitates. An interesting finding is that these “stars” did not show up using secondary electron detector when SEM accelerating voltage was below 20 kV, while apparent at energies above this level. Backscattered electron images did not show any features at the locations of precipitates indicating the non-particulate nature as is shown on the example of the 130-7 hot spot in Fig. 7.

Similar imaging of the cold spots did not indicate any of the dendritic objects present.

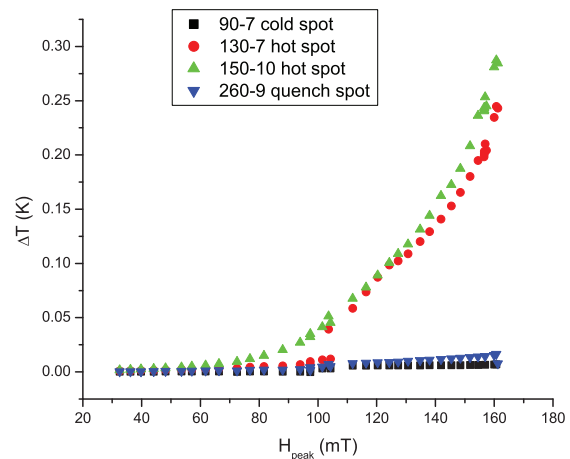


Figure 4: Temperature sensor readings versus peak magnetic field for two hot spots, one cold spot, and a quench site prior to the quench.

Energy dispersive X-ray spectroscopy (EDS) was performed at different spots on the “star” and around. Individual EDS energy spectra did not reveal any particular contamination, while EDS mapping showed a slightly higher oxygen concentration in the “border” area of the stars not apparent from individual spectra. It should be noted that EDS is not sensitive to any elements below atomic number of 12 (carbon), and hydrogen (a major element present in niobium) is not identified.

In order to investigate the nanoscale structure of the “stars”, Zeiss 1540XB FIB-SEM system at ANL Electron Microscopy Center was used to prepare TEM samples from the areas containing star branches. The area around the star was capped with the protective carbon layer of about 2  $\mu\text{m}$  thickness to preserve the near-surface structure throughout milling and thinning processes. Secondary electron images of several stages in the FIB sample preparation process are shown in Fig. 8. The analytical transmission electron mi-

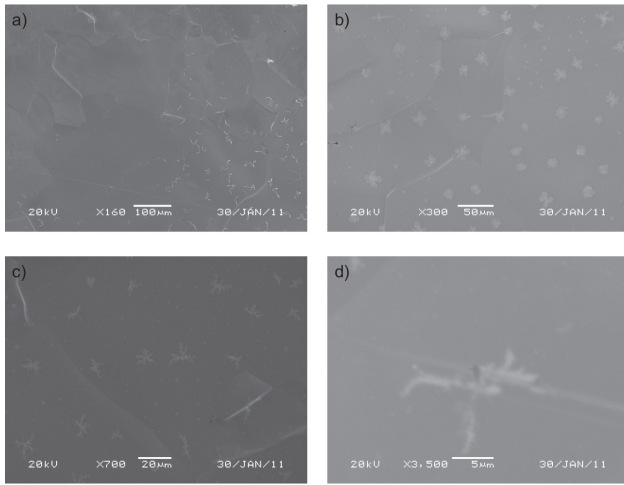


Figure 5: SEM secondary electron images of the dendritic objects found on the 130-7 hot spot cutout.

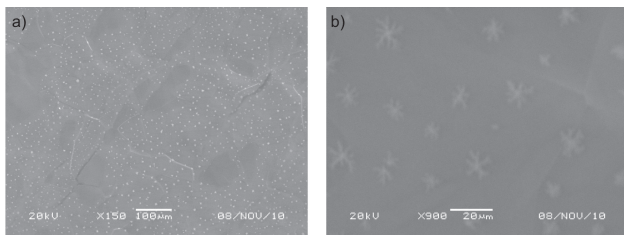


Figure 6: SEM secondary electron images of the dendritic objects found on the 150-10 hot spot cutout.

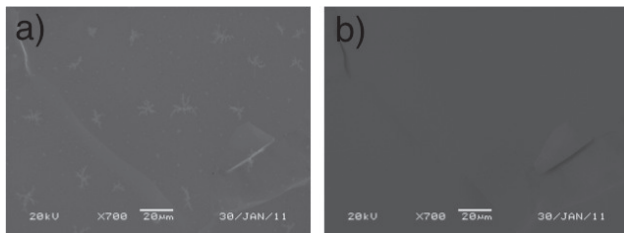


Figure 7: Secondary electron (a) and backscattered electrons (b) images of the same area covered with precipitates on the 130-7 hot spot cutout.

roscope FEI CM30T was used for imaging. The cross-sectional bright field TEM image of the area containing the precipitate is shown in Fig 9. Selected area diffraction patterns have been obtained from the precipitate (marked "1" in Fig. 9) and from niobium around (marked "2" in Fig. 9).

In addition to SEM/EDS and FIB/TEM studies, electron backscattered diffraction (EBSD) studies are on the way on the cutout samples and will be reported in another publication. Furthermore, comparative elastic recoil detection (ERD) measurements of the near-surface hydrogen distribution were performed on one of the cold spots and are reported in [9, 10].

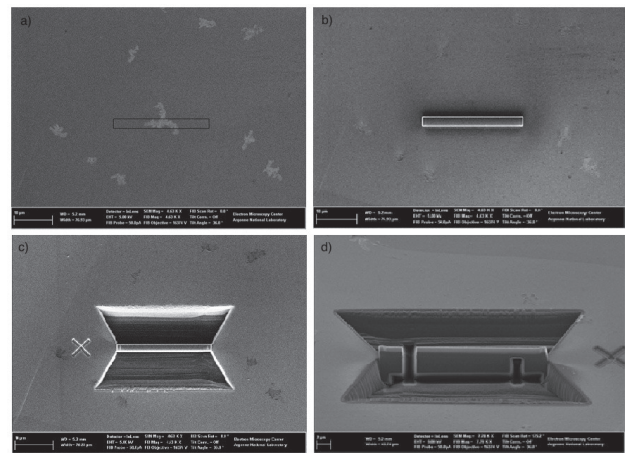


Figure 8: Steps in FIB preparation of site-specific sample for TEM: (a) area of carbon deposition marked by a ; (b) after carbon deposition; (c) after rough milling; (d) membrane ready to be extracted by omniprobe.

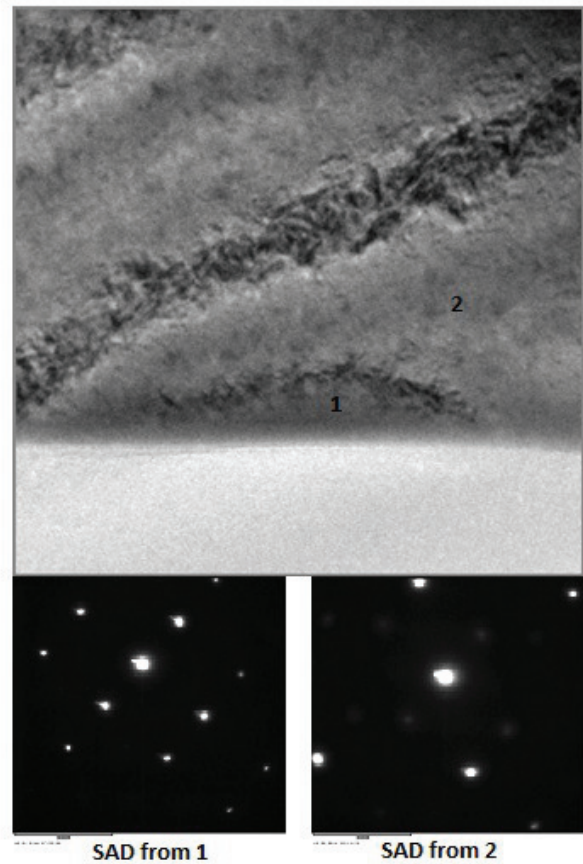


Figure 9: TEM image and selected area diffraction (SAD).

*Quench Location*

The high field quench happened at about 160 mT at the spot, which exhibited no extra pre-heating up to the quench field as shown in Fig. 4. This suggests that the character

of the quench in this cavity may have been mostly magnetic as opposed to many reported cases (see Ch. 5 in [11] for review) where local heating is observed starting from field levels far below the quench field leading to the thermal breakdown mechanism. A thorough SEM investigation of the quench location cutout revealed some surface features, which might have led to the quench. In Fig. 10 the black spots, which were found on the quench spot cutout, represent areas with the increased carbon content as detected by EDS. These are the only features we were able to identify

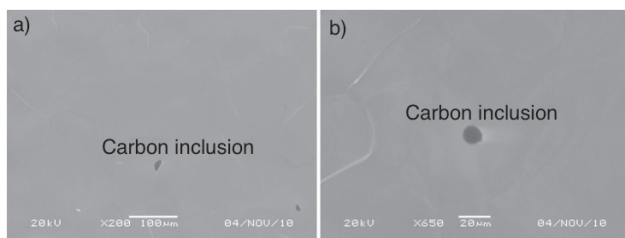


Figure 10: SEM images of the carbon inclusions found on the surface of the cutout from the quench site.

at this stage of surface investigations, which may have been the cause of the quench.

## DISCUSSION

Our findings of dendritic precipitates in two out of three hottest spots represent an interesting correlation of high field ( $> 100$  mT) RF losses with the particular microstructural features. Based on SEM/EDS results along with TEM imaging and diffraction we believe that the observed dendritic precipitates may be niobium hydrides similar to the ones reported in [12]. Similar objects were also observed by Vinnikov and Golubok [13] and their magnetic properties have been investigated. Our results indicate that the state of hydrogen precipitation may be of the importance for the high field performance of niobium cavities and require further investigations. The presence of dislocations and vacancies as hydride nucleation centers upon cooling down to 2 K may be a necessary condition for these hydrides to form. It is unclear at this point if hydrogen precipitation is connected to the high field Q-slope in any way, which is the subject of ongoing research. A search for inclusions, perhaps of a nanoscale size is currently under way on the high field Q-slope limited samples coming from a different unbaked cavity. Further details of the investigations and our findings on other samples will be published elsewhere.

For the high field quench site the only finding so far is a few carbon inclusions similar to the findings in [7] on the quench sites at lower surface fields. The carbon-enriched areas we observe are smaller than the ones in [7], which may be consistent with the much higher quench field in our experiment.

## ACKNOWLEDGEMENTS

The transmission electron microscopy and focused ion beam preparation was accomplished at the Electron Microscopy Center for Materials Research at Argonne National Laboratory, a U.S. Department of Energy Office of Science Laboratory operated under Contract No. DE-AC02-06CH11357 by UChicago Argonne, LLC. Authors would like to acknowledge Michael Morrone from Jefferson Lab for the help with the cavity test, and Hasan Padamsee from Cornell University for valuable discussions.

## REFERENCES

- [1] A. Grassellino. Muon spin rotation/relaxation studies of niobium for SRF applications. In *Proceedings of the 15th International Conference on RF Superconductivity*, 2011.
- [2] A. Romanenko and H. Padamsee. The role of near-surface dislocations in the high magnetic field performance of superconducting niobium cavities. *Superconductor Science and Technology*, 23(4):045008, 2010.
- [3] A. Romanenko. Crystalline microstructure role in the high-field Q-slope. In *Proceedings of 14th International Conference on RF Superconductivity*, 2009.
- [4] A. Romanenko. *Surface characterization of niobium cavity sections: understanding the high field Q-slope*. PhD thesis, Cornell University, 2009.
- [5] A. Romanenko. Review of high field Q-slope, surface measurements. In *Proceedings of the 12th Workshop on RF Superconductivity*, 2007.
- [6] A. Romanenko, H. Padamsee, G. Ereemeev, and J. Shu. Comparative surface studies on fine-grain and single crystal niobium using XPS, AES, EBSD and profilometry. In *Proceedings of PAC2007*, 2007.
- [7] X. Singer, S. Aderhold, A. Ermakov, W. Singer, K. Twarowski, M. Hoss, F. Schölz, and B. Spaniol. Surface investigation on prototype cavities for the European XFEL. In *Proceedings of the 1st International Particle Accelerator Conference*, 2010.
- [8] G. Ciovati. PhD thesis, Old Dominion University, 2005.
- [9] A. Romanenko and L. V. Goncharova. Investigation of near-surface interstitial hydrogen in cavity-grade niobium. In *Proceedings of the 15th International Conference on RF Superconductivity*, 2011.
- [10] A. Romanenko and L. V. Goncharova. Elastic recoil detection studies of near-surface hydrogen in cavity-grade niobium. *Superconductor Science and Technology*, 2011.
- [11] H. Padamsee. *RF Superconductivity: Volume II: Science, Technology and Applications*. Wiley-VCH, 2009.
- [12] M. L. Grossbeck and H. K. Birnbaum. Low temperature hydrogen embrittlement of niobium II - microscopic observations. *Acta Metallurgica*, 25:135–147, 1977.
- [13] L. Y. Vinnikov and A. O. Golubok. Direct observation of magnetic structure in niobium single crystals with hydride precipitate pinning centers. *Phys. Stat. Sol.*, 69:631, 1982.
- [14] W. Weingarten. On the dependence of the Q-value on the accelerating gradient for superconducting cavities. In *Proceedings of 13th Workshop on RF Superconductivity*, 2007.